CRYSTAL GROWTH & DESIGN

Article

pubs.acs.org/crystal

Structural Adaptation of Ni_4O_4 Units To Form Cubane, Open Dicubane, Dimeric Cubane, and One-Dimensional Polymeric Cubanes: Magnetostructural Correlation of Ni_4 Clusters

Debarati Das,[†] Goutam Mahata,[†] Amit Adhikary,[§] Sanjit Konar,[§] and Kumar Biradha*[,†]

[†]Department of Chemistry, Indian Institute of Technology, Kharagpur 721302, India

[§]Department of Chemistry, IISER Bhopal, Bhopal 462066, India

Supporting Information

ABSTRACT: The complexation reactions of a tripodal chelating ligand, [3,5-bis(2-amino-ethyl)-[1,3,5]triazinan-1-yl]-methanol (**L**), which is produced by the *in situ* transformation of 1,3,6,8-tetraazatricyclo[4.4.1.1^{3,8}]-dodecane (**L^1**) with $Ni(NO_3)_2{\cdot}6H_2O$ has been explored in the presence of ammonium salts of inorganic and organic anions. These reactions resulted in four crystalline complexes $[Ni_4(\mathbf{L})_2(\mu_3\text{-}OH)_2(NCS)_4]{\cdot}4H_2O$ (**1**), $[Ni_4(\mathbf{L})_2(\mu_2\text{-}N_3)_4(N_3)_2]{\cdot}2H_2O$ (**2**), $[Ni_8(\mathbf{L})_4(\mu_3\text{-}OH)_4(BDC)_3(H_2O)_4]{\cdot}BDC{\cdot}28(H_2O)$ (**3**, BDC = 1,4-benzene dicarboxylate) and $\{[Ni_4(\mathbf{L})_2(\mu_3\text{-}OH)_2(NDS)_2(H_2O)_2]{\cdot}NDS{\cdot}11(H_2O)\}_n$ (**4**, NDS = naphthalene-1,5-disulfonate). The crystal structure analyses of **1**−**4** reveal that all contain Ni(II) clusters, which act as secondary building units to generate higher order aggregates. The complexes **1**, **3**, and **4** contain exclusively Ni_4 cubane units: a discrete cubane in **1**, a dimer of cubanes linked by BDC in **3**, and cubanes linked in one dimension by NDS to form a 1D-coordination polymer in **4**. Interestingly, complex **2** exhibits an open dicubane with two missing vertices. Although a plethora of water molecules had been included in their crystal lattices, the crystals were found to be stable even at room temperature. The water molecules govern the overall crystal packing by the formation of strong hydrogen bonds and clusters. Large clusters of water such as $(H_2O)_{28}$ and $(H_2O)_{16}$ were observed in **3** and **4**, respectively, while dimers of water were observed in **1** and **2**. Magnetic susceptibility (χ_M) measurements in the temperature range of 2−300 K on **1**−**3** reveal that the metal centers are ferromagnetically coupled in all three depending on their respective exchange pathways. Interestingly, the room temperature (300 K) $\chi_M T$ values increase as the molecular aggregation increases from discrete cubane (5.5 cm^3 K mol^{-1}) to face sharing open dicubane (6.21 cm^3 K mol^{-1}) to connected dicubane (11.36 cm^3 K mol^{-1}). The modes of bridging by $^-$OH, N_3^-, and BDC and their bond angles with paramagnetic Ni(II) centers clearly explained the overall ferromagnetism operating in the spin clusters.

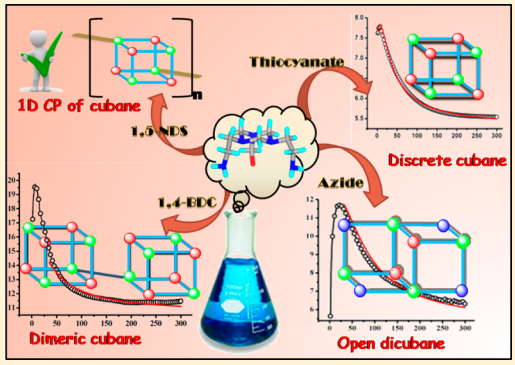

The past two decades have witnessed tremendous growth in the field of coordination chemistry in the form of polynuclear transition metal clusters, complex supramolecular architectures, and coordination polymers (CPs) via self-assembly processes involving metal salts and organic ligands.[1−3] These materials have a wide range of applications in various fields, such as adsorption, magnetism, molecular recognition, luminescence, nonlinear optics, and sensors.[4−13] The magnetic polymetallic discrete clusters of transition-metal ions have received much attention owing to their intriguing structural diversities and various applications as single molecule magnets and molecular refrigerators and in biological systems.[14−18] Among those clusters, tetranuclear cubane like $\{M_4O_4\}$ complexes [M = Cu, Ni, Co, etc.] are of particular interest for their interesting magnetic properties.[19−23] In these cubane clusters, the interaction between two paramagnetic metal centers are mediated by μ^3-O bridges originating from −OH, −OMe, or chelating ligands. In particular, for Ni_4O_4 clusters, the intracluster magnetic interactions were also shown to be fine-tuned by the use of multidentate bridging ligands, azide, thiocyanate, and cyanate ions.[24−29] Recently, Lin et al. have shown that coordination polymers can also be obtained by connecting the cubane unit via dicyanamide bridges.[30]

The creation of crystalline coordination polymers (CPs) by the process of self-organization of multiple small components is a fascinating area of research owing to their intriguing structures and functional properties.[4−13] The symmetrical disposition and number of coordination centers of an organic molecule and coordination geometry of the metal play a significant role in the overall symmetry of the structure and their properties.[31−34] The important task for the realization of predictable architectures is to transfer the molecular symmetry into supramolecular symmetry.[35−39] For example, a tetrahedral molecule such as hexamethylenetetraamine (HMTA) was shown to form diamondoid networks upon reaction with a

Received: May 29, 2015
Revised: July 3, 2015
Published: July 9, 2015

DOI: 10.1021/acs.cgd.5b00736
Cryst. Growth Des. 2015, 15, 4132−4141

linear dicopper spacer, $[Cu_2(OBz)_4]$ (OBz = benzoate), where the HMTA acts as a tetrahedral node.[40] In this paper, we present our studies on the complexes of [3,5-bis(2-aminoethyl)-[1,3,5]triazinan-1-yl]-methanol, **L**, a tripodal ligand that is obtained *in situ* from cage like molecule 1,3,6,8-tetraazatricyclo[4.4.1.1^{3,8}]dodecane, **L^1** during the course of the reaction (Scheme 1). Incidentally, **L^1** has the N atoms disposed

Scheme 1. Structural Drawings for [3,5-Bis(2-aminoethyl)-[1,3,5]triazinan-1-yl]methanol Anion (L) and 1,3,6,8-Tetraaza-tricyclo[4.4.1.1^{3,8}]dodecane (L^1)

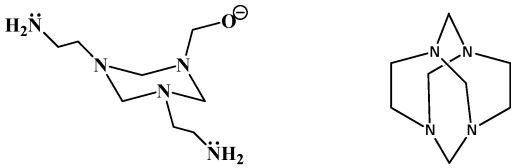

L **L^1**

in tetrahedral geometry similar to HMTA but does not possess a tetrahedral symmetry. We note here that although HMTA has over 650 crystal structures, including organic and inorganic, in Cambridge Structural Database (CSD),[41] the related molecule, **L^1**, has only two crystal structures to date; one is itself[42] and other is a cocrystal with hydroquinone.[43] Literature reports also reveal that ligand **L^1** is sensitive to various aromatic bases and forms several hexahydrotriazine derivatives.[44] In this paper, we present complexation studies of Ni(II) with **L**, which is generated *in situ* from **L^1** in the presence of ammonium salts of inorganic and organic anions. The analyses of the crystal structures of complexes reveal that **L** templates the formation of Ni_4O_4 cubane units, which can be linked to dimer and one-dimensional coordination polymers by using organic linkers such as 1,4-benzene dicarboxylate (BDC) and naphthalene-1,5-disulfonate (NDS). The crystal structures of four Ni(II) complexes of **L** are analyzed in detail in terms of hydrogen bonding and water clusters. Further, the studies on their magnetic properties reveal the correlation between the observed structures and ferromagnetic properties.

RESULTS AND DISCUSSION

The ligand **L^1** was prepared by condensation reactions of paraformaldehyde and ethylenediamine in DMF solvent.[45] The reaction of **L^1** with $Ni(NO_3)_2{\cdot}6H_2O$ in the aqueous NH_4SCN solution resulted in the single crystals of complex **1**, $[Ni_4(\mathbf{L})_2(\mu_3\text{-}OH)_2(NCS)_4]{\cdot}4H_2O$. Similarly, the repeat of this reaction in the presence of NH_4N_3 instead of NH_4SCN resulted in single crystals of complex **2**, $[Ni_4(\mathbf{L})_2(\mu_2\text{-}N_3)_4\text{-}(N_3)_2]{\cdot}2H_2O$. The crystal structure analyses of these complexes reveal that the ligand **L^1** transforms into a tripodal ligand **L** and anchors the faces of the Ni_4O_4 cubane moiety. In the case of complex **1**, discrete molecular structure resulted, which was further assembled by water molecules via hydrogen bonds to form a 2D network. Complex **2** was found to exhibit a face shared open dicubane, which was further assembled via strong hydrogen bonds with water molecules. With the intention of connecting the cubane units further, the organic ammonium salts of BDC and NDS were considered in place of SCN/N_3 ions, which resulted in crystals of complexes $[Ni_8(\mathbf{L})_4(\mu_3\text{-}OH)_4(BDC)_3(H_2O)_4]{\cdot}BDC{\cdot}28(H_2O)$ (**3**) and $\{[Ni_4(\mathbf{L})_2(\mu_3\text{-}OH)_2(NDS)(H_2O)_2]{\cdot}NDS{\cdot}11(H_2O)\}_n$ (**4**), respectively. As anticipated in **3** and **4**, the cubane units are linked by BDC and NDS to form a dimer of cubanes and a one-dimensional CP containing cubanes, respectively. Both complexes also contain uncoordinated BDC and NDS ions, which engage themselves in a plethora of hydrogen bonding with lattice water molecules to form 3D hydrogen bonded networks. The bridging of Ni(II) centers by O and N atoms prompted us to investigate the magnetic properties of the complexes **1**–**3** since they were all obtained in pure form and also in good yields. These studies revealed that the materials **1**–**3** exhibit ferromagnetic interactions and their susceptibility values depend on their respective structures. The detailed analyses of the cluster geometries and their linkages gave some insights into the observed magnetic properties. Pertinent crystallographic details for complexes **1**–**4** are given in Table 1, and bond lengths and angles around Ni(II) centers in crystal structures **1**–**4** are given in Tables 2–5, respectively. The N–H···O and N–H···N hydrogen bonding parameters in complexes **1**–**4** are given in Table 6. The O···O distances are given in Table 7.

Table 1. Crystallographic Parameters for Complexes 1, 2, 3, and 4

	1	2	3	4
structural formula	$C_{20}H_{50}N_{14}O_8S_4Ni_4$	$C_{16}H_{44}N_{28}O_4Ni_4$	$C_{64}H_{164}O_{56}N_{20}Ni_8$	$C_{36}H_{80}O_{29}N_{10}Ni_4S_4$
formula wt	977.82	927.63	2579.83	1480.18
temp (K)	293(2)	100(2)	100(2)	293(2)
λ (Å)	0.71073	0.71073	0.71073	0.71073
cryst syst	orthorhombic	triclinic	triclinic	triclinic
space group	*Fdd*2	$P\bar{1}$	$P\bar{1}$	$P\bar{1}$
a (Å)	24.015(2)	8.272(8)	10.820(1)	11.139(8)
b (Å)	35.730(3)	10.890(1)	13.024(1)	13.791(1)
c (Å)	8.780(7)	10.952(1)	19.095(2)	19.730(1)
α (deg)	90	65.671(2)	83.833(3)	97.262(2)
β (deg)	90	71.536(2)	83.869(2)	90.221(2)
γ (deg)	90	79.916(2)	85.987(3)	103.555(2)
V (Å^3)	7533.5(10)	851.5(1)	2655.4(4)	2921.1(4)
Z	8	1	1	2
ρ_{calcd} (g cm^{-3})	1.724	1.809	1.613	1.683
R_1 ($I > 2\sigma(I)$)	0.0329	0.0329	0.0440	0.0519
wR_2 (on F^2, all data)	0.0948	0.1330	0.1399	0.1652

DOI: 10.1021/acs.cgd.5b00736
Cryst. Growth Des. 2015, 15, 4132–4141

Table 2. Selected Bond Distances (Å) and Angles (deg) of Complex 1[a]

$Ni(1)-O(1W)_a$	2.046(3)	Ni(1)–Ni(1)	3.1700(7)
Ni(1)–O(1W)#	2.052(3)	Ni(2)–Ni(2)	3.1301(7)
Ni(2)–O(1W)	2.062(4)	$Ni(2)-O(11)-Ni(2)_a$	98°97′(12)
$Ni(1)-O(11)_a$	2.070(4)	$Ni(1)-O(11)-Ni(2)_a$	97°49′(14)
$Ni(2)-O(11)_a$	2.067(3)	Ni(1)–O(1W)–Ni(2)	94°69′(13)
$Ni(2)-O(1W)_a$	2.062(4)	Ni(1)–O(11)–Ni(2)	94°52′(12)
Ni(1)–Ni(2)#	3.0259(7)	Ni(1)–O(1W)–Ni(2)	98°39′(14)
$Ni(1)-Ni(2)_a$	3.1095(7)	$Ni(1)-O(1W)-Ni(1)_a$	101°34′(12)

[a]Sym operator a: 1/2 − *x*, 1/2 − *y*, *z*.

Table 3. Selected Bond Distances (Å) and Angles (deg) of Complex 2[a]

$Ni(1)-Ni(2)_b$	3.1908(6)	Ni(1)–N(10)	2.123(3)
Ni(1)–Ni(2)	3.0563(5)	$Ni(2)-N(10)_b$	2.153(3)
$Ni(2)-Ni(2)_b$	3.1081(6)		
Ni(1)–O(1)	2.040(2)	$Ni(1)-O(1)-Ni(2)_b$	102°50′(8)
Ni(2)–O(1)	2.064(2)	Ni(1)–O(1)–Ni(2)#	96°27′(9)
$Ni(2)-O(1)_b$	2.051(2)	$Ni(2)-O1-Ni(2)_b$	98°11′(8)
Ni(1)–N(7)	2.083(3)	Ni(1)–N(10)–Ni(2)	96°54′(11)
Ni(2)–N(7)	2.073(3)	Ni(1)–N(7)–Ni(2)	94°66′(11)

[a]Sym. transformation b: −*x*, 1 − *y*, 1 − *z*; # for differentiating similar atoms.

Table 4. Selected Bond Distances (Å) and Angles (deg) of Complex 3

Ni1–O1B	2.068(2)	Ni1–O1A–Ni2	97°41′(9)
Ni1–O4W	2.049(2)	Ni1–O4W–Ni4	97°78′(9)
Ni1–O1A	2.056(2)	Ni2–O3W–Ni4	93°56′(9)
Ni2–O1A	2.059(2)	Ni3–O4W–Ni4	100°14′(10)
Ni2–O1B	2.055(2)	Ni3–O3W–Ni4	101°85′(10)
Ni2–O3W	2.065(2)	Ni1–O4W–Ni3	93°42′(9)
Ni3–O1A	2.057(2)	Ni1–O1A–Ni3	93°89′(9)
Ni3–O4W	2.079(2)	Ni1–O1B–Ni2	97°16′(9)
Ni3–O3W	2.043(2)	Ni1–O1B–Ni4	97°08′(9)
Ni4–O1B	2.060(2)	Ni2–O1B–Ni4	93°31′(9)
Ni4–O4W	2.056(2)	Ni2–O3W–Ni3	98°67′(10)
Ni4–O3W	2.042(2)	Ni2–O1A–Ni3	98°41′(10)

Table 5. Selected Bond Distances (Å) and Angles (deg) of Complex 4

Ni1–O1W	2.057(3)	Ni1–O1W–Ni2	99°56′(12)
Ni1–O2W	2.040(3)	Ni1–O2W–Ni2	99°80′(12)
Ni1–O1A	2.067(3)	Ni1–O1A–Ni4	97°07′(10)
Ni2–O1W	2.038(3)	Ni1–O2W–Ni4	98°45′(10)
Ni2–O2W	2.048(3)	Ni2–O2W–Ni4	94°09′(11)
Ni2–O1B	2.062(3)	Ni1–O1W–Ni3#	94°08′(10)
Ni3–O1W	2.041(3)	Ni1–O1A–Ni3	93°04′(11)
Ni3–O4W	2.136(4)	Ni3–O1A–Ni4	99°69′(11)
Ni3–O1A	2.066(3)	Ni3–O1B–Ni4	98°87′(13)
Ni3–O1B	2.088(3)	Ni2–O1B–Ni4	93°11′(11)
Ni4–O2W	2.050(3)	Ni2–O1W–Ni3	100°19′(11)
Ni4–O1A	2.066(3)	Ni2–O1B–Ni3	97°89′(11)
Ni4–O3W	2.117(3)	Ni2–O2W–Ni4	94°09′(11)
Ni4–O1B	2.069(3)		

Discrete Ni_4O_4 Cubane Structure. The reaction of L^1 with $Ni(NO_3)_2{\cdot}6H_2O$ in the presence of ammonium thiocyanate in aqueous solution resulted in blue colored single crystals of complex **1**. It crystallizes in orthorhombic space group. The tripodal ligand (**L**) exhibits chair conformation and anchors one face (Ni_2O_2) of the Ni_4O_4 cubane via two

Table 6. Hydrogen Bonding Parameters in the Crystal Structures of 1–4[a]

complexes	interactions	H···A (Å)	D···A (Å)	D–H···A (deg)
1	$N-H\cdots N_a$	2.58	3.338(6)	143
	N–H···O	2.35	3.229(8)	166
2	$N-H\cdots N_b$	2.57	3.307(4)	140
		2.37	3.222(4)	159
	$N-H\cdots N_c$	2.31	3.064(4)	141
	$N-H\cdots O_d$	2.29	3.071(4)	145
3	$N-H\cdots O_e$	2.06	2.923(4)	160
		2.10	2.970(4)	161
	N–H···O(intra)	2.36	3.097(4)	139
	N–H···O(intra)	2.08	2.821(4)	139
		2.40	2.895(4)	115
		2.12	2.932(4)	150
4	$N-H\cdots O_g$	2.56	3.290(5)	139
		2.56	3.384(6)	153
	N–H···O (intra)	2.13	2.987(5)	158
		2.42	3.256(6)	155
	N–H···O (intra)	2.30	3.089(7)	145
		2.45	3.181(6)	138
	N–H···O (intra)	2.25	3.049(5)	148
	$N-H\cdots O_f$	2.39	3.248(7)	160
	N–H···O (intra)	2.46	3.216(5)	142

[a]Sym. Transformation: (c) −*x*, 1 − *y*, −*z*; (d) −1 + *x*, *y*, *z*; (e) −*x*, 2 − *y*, −*z*; (f) 1 − *x*, 1 − *y*, 1 − *z*; (g) 1 − *x*, 1 − *y*, −*z*.

Table 7. Other Intermolecular Interactions (Å) of Complexes 1–4

Complexes	Interactions	Distances	Interactions	Distances
1	$O_w\cdots O_w$	2.816(12)		
2	$O_w\cdots O_w$	2.876(6)		
3	$O_w\cdots O_w$	2.745(4)	$O_w\cdots O_{anion}$	2.751(4)
		2.735(4)		2.763(3)
		2.820(4)		2.793(4)
		2.713(4)		2.852(4)
		2.881(5)		
		2.744(4)	$O_w\cdots O_{coord\text{-}anion}$	2.698(3)
		2.780(4)		2.838(4)
		3.065(4)	$O_{coord\text{-}w}\cdots O_w$	2.794(4)
		2.846(5)		2.751(4)
		2.721(4)		3.375(4)
		2.824(5)		
		2.847(4)		
		2.903(5)	$O_{bridg\text{-}OH^-}\cdots O_w$	2.832(3)
		2.771(4)		3.007(4)
		2.781(5)		
		2.802(5)		
4	$O_w\cdots O_w$	2.806(6)	$O_w\cdots O_{anion}$	2.755(7)
		2.755(15)		2.778(7)
		2.779(12)		2.806(7)
		2.759(14)		2.862(9)
		2.870(2)		2.862(9)
		2.410(2)		2.846(7)
		2.930(2)		2.770(6)
		2.900(2)		2.750(12)
		2.380(3)		2.828(19)
	$O_{bridg\text{-}OH^-}\cdots O_w$	2.890(5)	$O_{coord\text{-}w}\cdots O_w$	2.867(6)
		3.186(5)		3.114(6)

DOI: 10.1021/acs.cgd.5b00736
Cryst. Growth Des. 2015, 15, 4132–4141

ethylenediamine-like chelating interactions with two Ni(II) centers, and also the pendent O atom of **L** participates in the Ni_2O_2 core, which exhibits μ^3-coordination. The second O atom of the Ni_2O_2 face comes from OH^-, which also exhibits μ^3-coordination. All of the Ni(II) centers exhibit octahedral coordination geometry as they coordinate with three N atoms and one O atom from the **L** and one each of anion (SCN) and OH^-. The distances for Ni···Ni separations were found within the Ni_4 tetrahedron to be 3.0259(7), 3.1301(7), 3.1095(7), and 3.1700(7) Å. The angle between Ni−O−Ni involving μ^3-O atom from the ligand is 98°97′(12) whereas the angle Ni−O−Ni involving OH^- shows a comparatively larger angle, 101°34′(12) (upper face of the cube in Figure 1b). In the

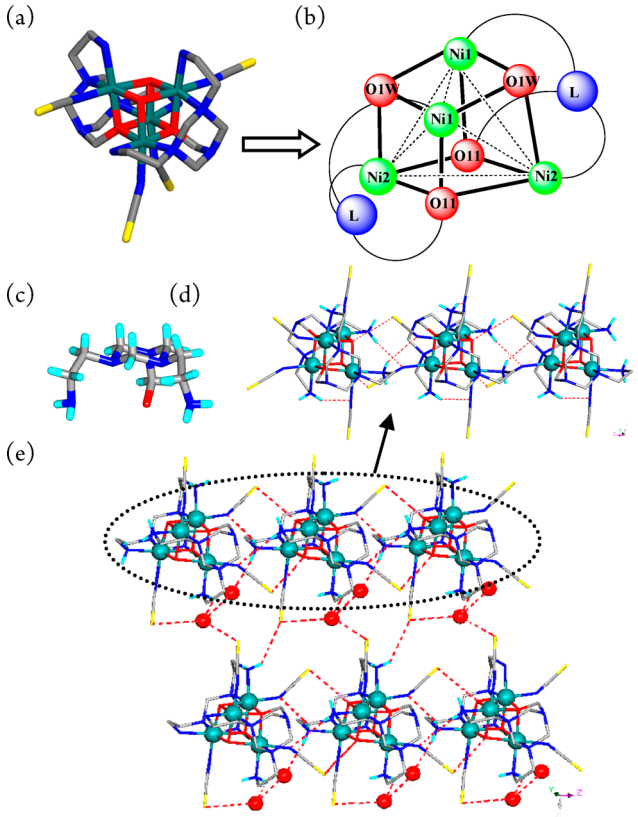

Figure 1. Illustrations for the crystal structure of **1**: (a) cubane unit with anions and **L** (H atoms are omitted for clarity); (b) Ni_4 tetrahedron residing in Ni_4O_4 SBU; (c) chair conformation of **L**; (d) inter- and intramolecular H-bonding interactions in the 1D chain; (e) 2D-hydrogen bonding layer of cubane units; notice 1D chains via O−H···S and N−H···NCS (hydrogen atoms are omitted for clarity).

other faces, where O atoms come from both water and ligand, Ni−O−Ni angles show a slight deviation from perfect 90° (Table 2). The N−H···NCS (N···N = 3.543(6) Å) and μ^3-O−H···SCN (O···S = 3.344(3) Å) hydrogen bonding interactions connect the cubane units to form a 1D-chain along the *c*-axis (Figure 1d). The NH_2 of the ligand also exhibits N−H···N (N···N = 3.338(6) Å) hydrogen bonding with the coordinated SCN^- in intramolecular fashion. The dimer (O_w···O_w = 2.816(12) Å) of water molecules joins the 1D chains further via O_w−H···SCN (O···S = 3.303(8) and 3.403(11) Å) and N−H···O_w (N···O = 3.229(8) Å) hydrogen bonds to form a 2D network (Figure 1e). The observed Ni_4O_4 cubane structure gave an idea that indeed it is possible to generate CPs containing Ni_4O_4 units as SBUs by using inorganic/organic dianions, in place of SCN^-, which act as linkers between the metal centers.

Face-Sharing Dicubane with Two Missing Vertices. It was anticipated that the replacement of SCN in **1** by an azide ion will result in the linking of cubanes to form CPs because azide ion is known as good linker between the metal centers via various binding modes (Scheme 2). Therefore, the reaction was

Scheme 2. Possible Binding Modes of Azido Ligand

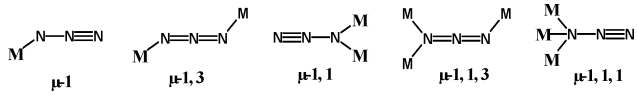

repeated by following similar conditions but by replacing NH_4SCN with NH_4N_3. Single crystal analysis of the resultant crystal reveals an interesting structure that contains the same tripodal ligand, **L**, which anchors a dicubane with two missing vertices. The single crystals of **2** exhibit $P\bar{1}$ space group. The azide ion does not act as a bridge between clusters because it exhibits μ-1 and μ-1,1 binding modes.

The dicubane unit is constituted by $Ni_4N_4O_2$ unit; the N atoms and O atoms in this cluster belong to azide and **L**, respectively. The ligand **L** binds the two Ni(II) centers in a similar fashion to that of the previous structure. The Ni(II) centers exhibit octahedral geometry because they coordinate to two O atoms of the ligand and four N atoms, two each from **L** and azide ions. The previous structure contains a Ni_4 tetrahedron, while the present structure contains a Ni_4 rhomboid with side distances of 3.0563(5) and 3.1908(6) Å between Ni(II) centers (Figure 2b). The shorter and longer

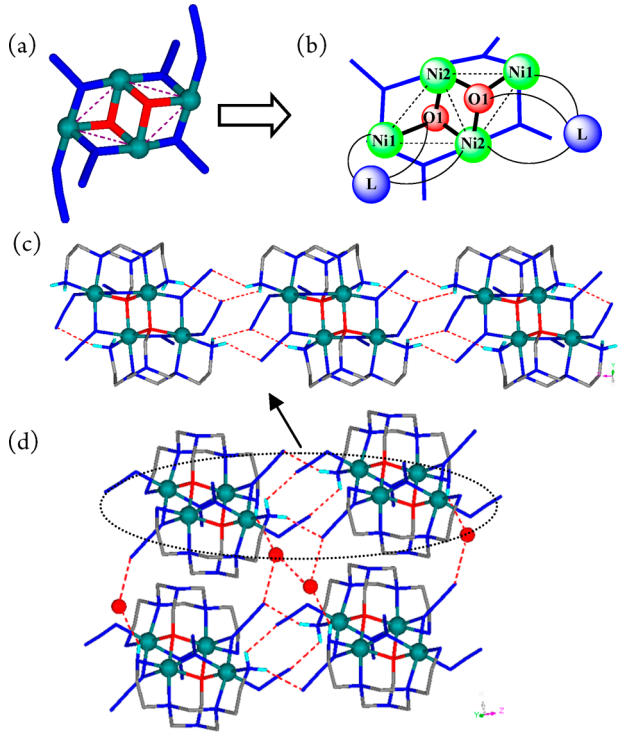

Figure 2. Illustrations for the crystal structure of **2**: (a) open dicubane unit; two types of binding modes of azide are shown; (b) open dicubane structure depicted with L_2Ni_4 rhomboid shown by dotted lines; (c) 1D chain formed via hydrogen bonding; (d) 2D hydrogen bonded network.

DOI: 10.1021/acs.cgd.5b00736
Cryst. Growth Des. 2015, 15, 4132−4141

diagonals exhibit Ni···Ni distances of 3.1081(6) and 5.421 Å, respectively. A one-dimensional chain results via intermolecular N−H···N_3^- hydrogen bonding (N···N = 3.064(4) and 3.353(5) Å), whereas intramolecular N−H···N_3^- hydrogen bonding (N···N = 3.222(4) Å) with the nonbridging azide anion also exists in the cluster (Figure 2c). The 1D chains further aggregated via hydrogen bonding of bridged azide ions and NH_2 groups with the dimer of water molecules [N···O = 3.047(5) and 3.071(4) Å, O···O = 2.876(6) Å] to form a two-dimensional layer (Figure 2d).

Dicubane by Connecting with a Linear Linker. 1,4-Benzene dicarboxylate (BDC) is known as a good dianionic organic linker and also to form several metal clusters.[46−50] Therefore, it was anticipated that the linking of the cubanes that is observed in complex **1** would result in the formation of a diamondoid network in which cubanes serve as tetrahedral nodes and BDC units serve as linkers. The reaction of the ammonium salt of BDC, ligand $\mathbf{L}^1$, and $Ni(NO_3)_2{\cdot}6H_2O$ in water resulted in the single crystals of complex **3**.

The crystal structure analysis reveals that a similar cubane unit persisted in the complex; however the cubane units are not linked to infinite arrays as anticipated. The geometry of **L** and coordination geometry of Ni(II) are similar to those observed in the crystal structure of **1**. In **3**, the BDC dianions can be categorized as three types depending on their coordination: one acts as a bilinker, one coordinates only with one of the two $-COO^-$ groups, and the third one does not coordinate to Ni(II). As a result, only two cubane units are linked together by the BDC to form a dicubane in which the cubanes are separated by 11.615 Å (Ni3···Ni3). The dicubane clusters are linked further by extensive hydrogen bonding between **L**, coordinated and free water molecules, and carboxylates of BDC. The ligand, coordinated water molecule, and BDC also participate in intramolecular hydrogen bonding (N···O = 3.097(4), 2.821(4), and 3.485(4) Å). The dicubane units are interlinked via two N−H···OOC (N···O = 2.923(4) and 2.821(4) Å) and one O−H···OOC (O···O = 2.740(4) Å) hydrogen bonds with coordinated water molecules to form a 1D-zigzag chain along the *a*-axis (Figure 3d). Free terephthalate ions (O···O = 2.932(4) and 2.970(4) Å) (Figure 3c) and H_2O connect these chains into a three-dimensional network via a plethora of hydrogen bonds (Figure 3c). Interestingly, it can be seen that the free BDC anions are surrounded by H-bonded water molecules, which form a one-dimensional column along the *a*-axis with a repeat unit of a $(H_2O)_{28}$ cage (Figure 3f). In this repeat unit, ten molecules have hydrogen bonds only with water itself, while 18 molecules interact with water and the walls of the channels. In the column of water molecules, 18 molecules out of 28 are involved in the formation of a cage, whereas ten molecules just dangle around the column and interact with the walls of the channels. The cage-like repeat unit can be described as the fused rings of four five-membered and two six-membered rings. The water clusters are connected by a water tetramer to give a continuous column of water molecules (Figure 3g).

Cubane to Infinite One-Dimensional Coordination Polymer. Because sulfate ions are known to weakly coordinate to metal centers, NDS was considered as a linker in order to produce higher dimensional networks containing cubane as a SBU. Accordingly, the $Ni(NO_3)_2{\cdot}6H_2O$ and ligand $\mathbf{L}^1$ were reacted in the presence of ammonium naphthalene-1,5-disulfonate. This reaction resulted in the blue colored single crystals of complex **4**. The crystal structure analysis reveals that

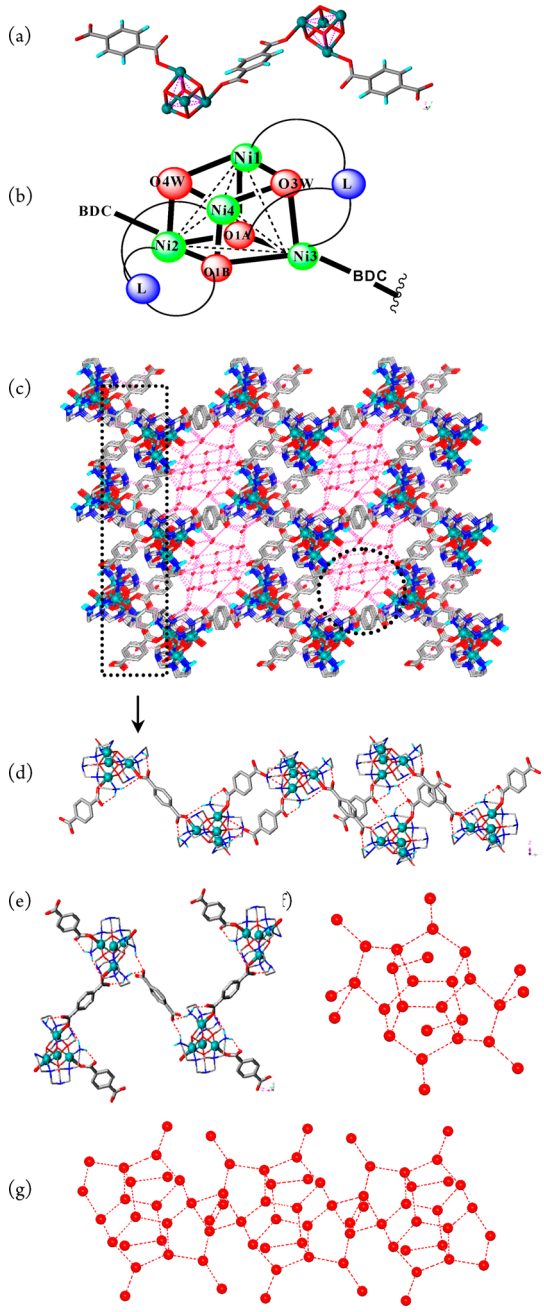

Figure 3. Illustrations for the crystal structure of **3**: (a) dicubane unit connected by a bridging terephthalate; (b) Ni_4O_4 cubane with labeling; (c) 3D network: presence of water cluster surrounding in 3D channels shown here; (d) 1D zigzag chain formed by N−H···O and O_w−H···O hydrogen bonding; (e) free BDC connecting the clusters via hydrogen bonding; (f) repeat unit of water clusters; (g) water clusters forming a continuous column.

recurrence of the formation of **L** and cubane units similar to **1** and **3**. In the cubane, two of the four Ni(II) corners are connected by NDS ions and the other two corners are connected by H_2O molecules. As a result, NDS links the cubane units into a linear one-dimensional CP (Figure 4e). Apart from coordination linkages, the one-dimensional chains also contain N−H···O (N···O = 3.216(5), 3.049(5), 3.089(7), 2.987(5), and 3.543(5) Å) hydrogen bonds between sulfonates and $-NH_2$ of the ligand. These one-dimensional CPs are linked further via hydrogen bonding between $-NH_2$ and sulfonates

DOI: 10.1021/acs.cgd.5b00736
Cryst. Growth Des. 2015, 15, 4132−4141

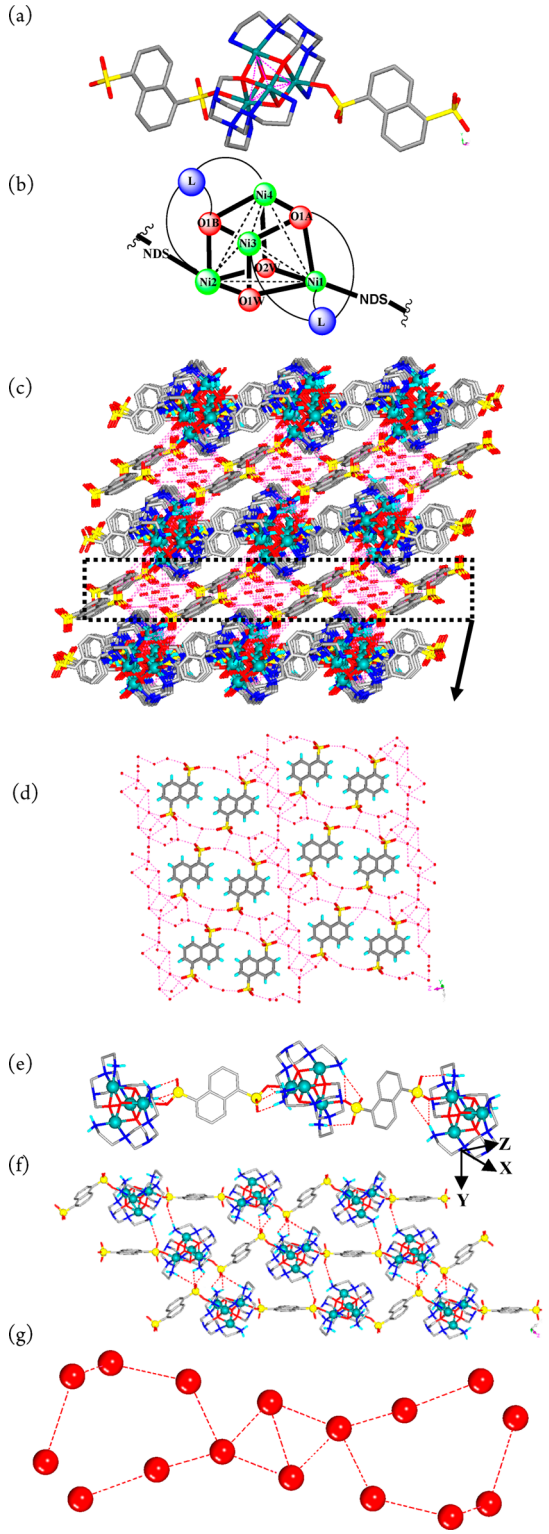

Figure 4. Illustrations for the crystal structure of **4**: (a) single cubane unit with anions and **L** (hydrogen atoms are omitted for clarity); (b) Ni_4O_4 cubane with labeling; (c) 3D network (hydrogen atoms are omitted for clarity); (d) hydrogen bonded network of acid and water column; (e) formation of 1D coordination polymer, intramolecular H-bonds are also shown; (f) formation of 2D layer by N−H···O between the 1D chains; (g) $(H_2O)_{16}$ water cluster.

(N···O = 3.290(5) Å) to form 2D layers (Figure 4f). Between such 2D layers of CPs there exists a 2D layer of anion and H_2O molecules; in these layers the dimers of the NDS anions are surrounded by a plethora of water molecules via O−H···O hydrogen bonds (Table 7), which are formed between the water molecules themselves and water and sulfonates (Figure 4d). In summary, this structure can best be described as a bilayer structure containing alternate hydrophobic and hydrophilic layers along the *b*-axis with interlayer separation of hydrophobic/hydrophilic layers of 13.8 Å. These layers are hydrogen bonded with each other via a plethora of strong hydrogen bonds between $-NH_2$, bridged −OH, coordinated H_2O and O atoms of sulfonates.

A water cluster formed by 16 free water molecules, eight independent, was found within the layer. The geometry of the cluster can be described as a cyclic tetramer in which the corners are attached to the water chains of two and four water molecules(Figure 4g). The crystal structures of **3** and **4** indicate that water molecules play crucial roles in assembling these clusters and 1D chains further via strong hydrogen bonds.

UV−Vis−NIR Solid State Diffusion Reflectance Spectra. The diffuse reflectance spectra of **1**, **2**, and **3** were recorded in the 200−1400 nm region and are shown in Figure S2, Supporting Information. The bands in the vicinity of 250 nm for all the complexes are ascribed to intraligand charge-transfer transitions (n to σ^* transition). The absorption bands observed at around 380 nm for the complexes have been assigned as $^3A_{2g}$ to $^3T_{1g}$ (P) transition, and broad peaks at around 610 nm for all the complexes are attributed to $^3A_{2g}$ to $^3T_{1g}$ (F) transition, whereas bands at 979, 1030, and 1006 nm for **1**−**3**, respectively, are attributed as $^3A_{2g}$ to $^3T_{2g}$ (F) transitions.[51,52] The additional peak at 309 nm for complex **2** is probably due to charge transfer of azide groups to Ni centers. This assignment gives rise to the energy parameters, Dq values of 1021, 971, and 994 cm^{-1} for **1**−**3**, respectively, which are characteristic of octahedral nickel(II). The nephelauxetic parameter (β) for all the complexes indicates a significant covalent character of the nickel(II) complex (Table S1, Supporting Information).

Magnetic Properties. The variable-temperature magnetic susceptibility data for complexes **1**−**3** were collected in the temperature range of 1.8−300 K under a field of 0.1 T. The DC susceptibilities are shown in the form of $\chi_M T$ (χ_M is molar magnetic susceptibility) as a function of temperature. All the *J* terms in the Hamiltonian equations represent exchange coupling constant or exchange interaction; *S* terms are spin angular momentum operators, and μ_B is the Bohr magneton.

Discrete Cubane. The magnetic behavior of **1** is illustrated in Figure 5. The $\chi_M T$ value of 5.52 cm^3 K mol^{-1} at room temperature is higher than the expected value for four uncorrelated Ni(II) ions with g = 2 (4 cm^3 K mol^{-1}). A high experimental susceptibility value can be explained considering ferromagnetic interactions among the metal centers and/or orbital contribution of the metal. Upon cooling, $\chi_M T$ continuously increases and reaches a maximum of 7.7 cm^3 K mol^{-1} at 10 K, close to the expected value for an S = 4 ground state with a g value of 2.29. This feature indicates dominant intracluster ferromagnetic interactions. Below 10 K, the $\chi_M T$ product slowly decreases, due to zero field splitting (ZFS)[26,30,53−56] or to the presence of weak antiferromagnetic intercluster interactions. Moreover, it has been recently shown from a structural point of view that an explanation of magnetic exchange can be given considering the Ni−O−Ni angle.[26,57,58] A ferromagnetic interaction can be observed if the Ni−O−Ni angle is close to orthogonality, and antiferromagnetism results if the bridging angle is greater than 99°. The experimental $\chi_M T$

DOI: 10.1021/acs.cgd.5b00736
Cryst. Growth Des. 2015, 15, 4132−4141

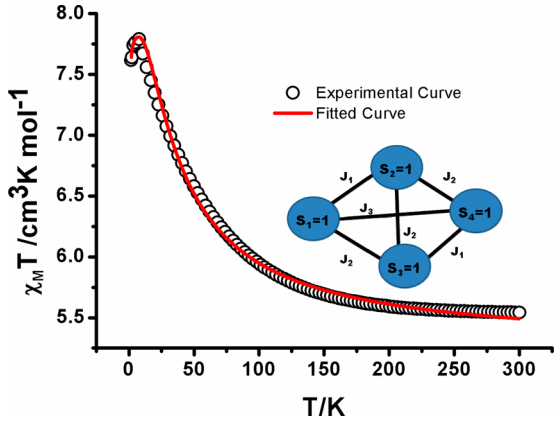

Figure 5. Illustrations for magnetic measurement of **1**: temperature dependence of $\chi_M T$ measured at 0.1 T; the red solid line is the best fit obtained along with the model used for the data fitting of **1**; balls represent metal centers, and lines represent connectivity between two metal centers.

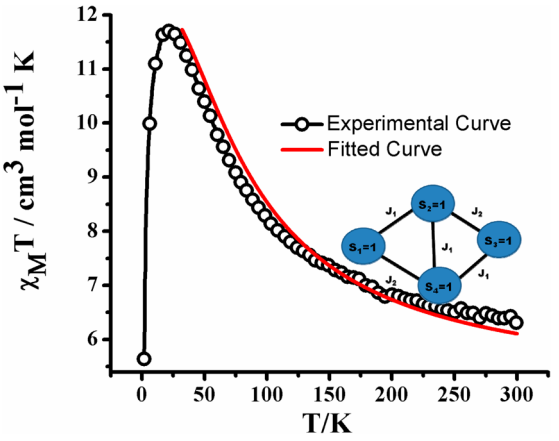

Figure 6. Illustrations for magnetic measurement of **2**: temperature dependence of $\chi_M T$ measured at 0.1 T. The red solid line is the best fit obtained along with the model used for the data fitting of **2**.

vs T plot was fitted using the Hamiltonian in eq 1 based on the model given in the inset of Figure 5.

$$H = -J_1(S_1S_2 + S_3S_4) - J_2(S_1S_3 + S_2S_3 + S_2S_4) - J_3(S_1S_4) - g\mu_B H \sum_{i=1}^{4} S_i \quad (1)$$

The best fit afforded g = 2.29, J_1 = +14.9 cm^{-1}, J_2 = +0.30 cm^{-1}, and J_3 = −0.95 cm^{-1}, which suggests the presence of dominant ferromagnetic interactions along with a weak antiferromagnetic interaction among the metal centers in **1**. J_1 represents coupling constants where the Ni−O−Ni angle is less than 99°, and J_2 represents coupling constants where Ni−O−Ni angle is greater than 99°. The antiferromagnetism is contributed by that face where both O atoms come from μ^3-OH$^-$ (Ni−O−Ni is 101°34′(12)).

The magnetization curve at 2 K shows a continuous increase up to the saturation value of 8.64μ_B, which corresponds well to a ground-state spin S = 4, in agreement with the $\chi_M T$ data and is also indicative of strong ferromagnetic interaction because at the strong external field it attains saturation (Figure S8a, Supporting Information). Adapting the Curie−Weiss equation, $\chi_M = C/(T - \theta)$, magnetic susceptibility values are further analyzed. The Curie−Weiss law is obeyed almost perfectly except at low temperature where some amount of zero-field splitting applies (Figure S9a, Supporting Information). The positive value of Weiss constant (θ) also indicates the presence of ferromagnetism in the complex (θ = +6.87 K).

Face Sharing Open Dicubane. The thermal variation of the product of the molar magnetic susceptibility per Ni(II) tetramer and temperature ($\chi_M T$) for the open cubane structure shows a room temperature value of 6.21 cm^3 K mol^{-1}, which is higher than expected for four exchange-free Ni(II) (for S = 1) ions with g = 2 (Figure 6). The high experimental susceptibility value can be explained considering ferromagnetic interactions among the metal centers or orbital contribution of the metal. On lowering the temperature, the $\chi_M T$ value shows a gradual increase to reach a maximum value of 11.76 cm^3 K mol^{-1} at 20.49 K. Below this temperature, the value decreases to reach 5.64 cm^3 K mol^{-1} at 2.53 K. This nature of the curve clearly indicates that **2** also exhibits dominant ferromagnetic interactions between the Ni(II) centers. The decrease observed at low temperatures is due to a zero field splitting (ZFS) of the S = 4 ground spin state. The dicubane core consists of the nickel ions bridged by combinations of μ^3-O$^-$ and $\mu^{1,1}$-N$_3$, which incidentally create the exchange pathways. As a result, there are five connections within the cluster that will contribute to the exchange pathway. The longest diagonal has been avoided due to very weak interaction (Ni···Ni = 5.421 Å). The end-on bridging azide ions influences the ferromagnetic interaction over a small antiferromagnetic coupling that can be expected (Ni−O−Ni = 102°50′(8)) in the cluster.[59−61] The magnetic interactions are modeled taking symmetry related units into consideration with the Hamiltonian written as eq 2 and the model given in inset of Figure 6. The best fitting is obtained by considering the following parameters: J_1 = +36 cm^{-1}, J_2 = +15 cm^{-1}, and g = 2.22. Positive value of J suggests dominant ferromagnetic interactions through both J_1 and J_2 exchange pathways. The magnetization plot, shown in Figure S8b, Supporting Information, is analogous to that of **1** and in agreement with the ferromagnetic coupling. The Curie−Weiss plot deviates from linearity at low temperature due to the presence of dominant ZFS in the complex (Figure S9b, Supporting Information). The Curie−Weiss constants are +5.875 cm^3 K mol^{-1} and +27.685 K; the positive value of θ indicates strong ferromagnetism.

$$H = -J_1(S_1S_2 + S_3S_4 + S_2S_4) - J_2(S_1S_4 + S_2S_3) - g\mu_B H \sum_{i=1}^{4} S_i \quad (2)$$

Dimeric Cubane. The carboxylate group is most widely used as a linker to generate polynuclear complexes with interesting magnetic properties. However, terephthalate facilitates antiferromagnetic interactions.[62−65] The temperature dependency of magnetic susceptibility has been shown in Figure 7. The parabolic decrease in value of $\chi_M T$ from 19.74 cm^3 K mol^{-1} at 7.33 K to 11.45 cm^3 K mol^{-1} at room temperature clearly indicates the presence of ferromagnetic coupling between Ni^{2+} ions since the value is slightly higher than the expected value 9.94 cm^3 K mol^{-1} at room temperature for eight isolated Ni^{2+} ions (g = 2.2). The high experimental susceptibility value can be explained considering ferromagnetic interactions among the metal centers or orbital contribution of metal. In the cubane unit, a similar type of μ^3-OH$^-$ mediated ferromagnetic

DOI: 10.1021/acs.cgd.5b00736
Cryst. Growth Des. 2015, 15, 4132−4141

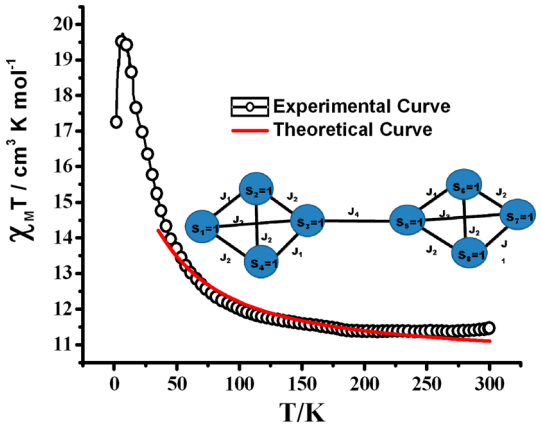

Figure 7. Illustrations for magnetic measurement of **3**: temperature dependence of $\chi_M T$ measured at 0.1 T along with the model.

superexchange interactions as that of **1** can be seen. The magnetic behavior was investigated, applying the Hamiltonian given as eq 3. A nice fit of the data gave J_1 = +18.9 cm^{-1}, J_2 = +0.20 cm^{-1}, J_3 = −0.95 cm^{-1}, J_4 = −0.10 cm^{-1}, and g = 2.29. The negative values of exchange pathways J_3 and J_4 can be attributed to Ni−O−Ni angle of 101°71′(17) and a negligible intercluster antiferromagnetic interaction.

The M/N μ_B vs H plot shows a saturation of 8.97μB at 2 K and supports overall ferromagnetic behavior of the complex (Figure S8c, Supporting Information). The complex satisfies Curie−Weiss law well; deviation at low temperature is attributed to ZFS present in the system like in complex **1**(Figure S9c, Supporting Information). Similarly, the positive Curie constant (+6.146 cm^3 mol^{-1} K) and Weiss constant, θ (+7.421 K), values indicate ferromagnetism like previous complexes.

$$H = -J_1(S_1S_2 + S_3S_4 + S_5S_6 + S_7S_8) - J_2(S_1S_4 + S_2S_3 + S_2S_4 + S_5S_8 + S_6S_7 + S_6S_8) - J_3(S_1S_3 + S_5S_7) - J_4(S_3S_5) - g\mu_B H \sum_{i=1}^{4} S_i \quad (3)$$

CONCLUSIONS

The complexation capability of a tripodal *in situ* generated ligand **L** was explored and shown to be capable of templating Ni(II) clusters on consistent basis. The cage-like ligand **L**^{1} was found to be transformed into the chelating ligand in the presence of ammonium salts, which can be linked to top down *in situ* synthesis of a ligand. Further, our efforts to isolate **L** by treating **L**^{1} with NH_4OH were unsuccessful due to the formation of mixtures. From this, it can be stated that ammonium salts help the breaking process, while the presence of Ni(II) ions controls such breaking process by trapping in situ the generated **L**. The presence of SCN^- anion templated a single cubane structure, while the presence of N_3^- anion templated an open dicubane structure. The use of organic anions such as NDS and BDC resulted in the linking of Ni_4O_4 cubane units to a dimer and a polymer, respectively. The bridging of the metal centers by the ligand resulted in magnetic coupling. The studies on magnetism of complexes **1**−**3** revealed dominating ferromagnetic interaction in all the clusters. The solvent molecules took part in hydrogen bonding with the ligand and cubane unit to propagate higher-dimensional networks. We note here that previously 1,3,5-triazacyclohexane containing -OMe and -NMe_2 tethers were shown to form face capped Cu_3Br_3 clusters but were not shown to form cubane-like M_4O_4 clusters.[66] Further, it was also shown to form an open cubane containing Co_3O_4 cluster in which the Co(II) corners are capped by triazacyclohexanes.[67] Interestingly, it was reported that Ni_4O_4 or Co_4O_4 cubanes can be linked to 3D networks, which also exhibited paramagnetic interactions in a similar way to the ones observed here.[30] Interestingly, the room temperature (300 K) $\chi_M T$ values were found to increase as the molecular aggregation increases from discrete cubane (5.5 cm^3 K mol^{-1}) to face sharing open dicubane (6.21 cm^3 K mol^{-1}) to connected dicubane (11.36 cm^3 K mol^{-1}). These values are comparable to literature reported values of Ni_4O_4 cubanes (Tables S2−S4, Supporting Information). The modes of bridging by $^-$OH, N_3^-, and BDC and their bond angles with paramagnetic Ni(II) centers clearly explained the overall ferromagnetism operating in the spin clusters. Further studies in our laboratory are in progress to link the cubane units into higher dimensional networks using organic linkers and explore their magnetic properties.

EXPERIMENTAL SECTION

All the chemicals, such as paraformaldehyde, ethylenediamine, nickel(II) nitrate, and *N*,*N*-dimethylformamide, were purchased from local chemical suppliers and used without purification. Ammonium salts of all linkers were prepared from their corresponding sodium salts. Elemental analyses (C, H, and N) were performed with a PerkinElmer model 240C elemental analyzer. FTIR spectra were recorded with a PerkinElmer Instrument Spectrum Rx serial no. 73713. The purity of bulk of complexes **1**−**3** was determined by PXRD using a Bruker AXS X-ray diffractrometer (40 kV, 20 mA) using Cu Kα radiation (λ = 1.5418 Å) over the 5−50° (2θ) angular range and a fixed-time counting of 4 s at 25 °C. TGA was recorded in a PerkinElmer instrument, Pyris Diamond TG/DTA. The diffuse reflectance spectra (DRS) were recorded with a Cary model 5000 UV−vis−NIR spectrophotometer. Magnetic measurements were performed using a Quantum Design SQUID-VSM magnetometer. The measured values were corrected for the experimentally measured contribution of the sample holder, while the derived susceptibilities were corrected for the diamagnetism of the samples, estimated from Pascal's tables.[68]

Synthesis of Metal Complexes. All the complexes have been prepared by direct mixing technique in aqueous medium adding three components, ligand, ammonium salt of linkers, and $Ni(NO_3)_2{\cdot}6H_2O$. The complexation reactions with other metal salts gave only precipitates.

Preparation of Complex ***1***. A mixture of **L**^{1} (0.017 g in 2 mL of H_2O, 0.1 mmol) and a 0.2 mmol solution (0.0192 g in 2 mL of distilled water) of NH_4SCN was mixed with $Ni(NO_3)_2{\cdot}6H_2O$ solution (0.0272 g in 2 mL of H_2O, 0.092 mmol), and the resultant solution was warmed to 60 °C to dissolve the contents. The dark blue crystals were obtained by slow evaporation and dried in air. Yield: 30% based on **L**^{1}. Elemental analysis (%) Calcd for $C_{20}H_{50}N_{14}O_8S_4Ni_4$: C 25.01, H 4.81, N 20.10. Found: C 24.99, H 4.78, N 20.05. IR, KBr (cm^{-1}): 3494.64(b), 3337.44(wb), 2865.73(b), 2373.41(w), 2082.30($\upsilon_{C\text{-}Nstrt}$), 2063.87(w), 1601.62($\upsilon_{C=C}$, b), 1284.12(m), 1220.61(s), 1112.91(s), 1036.10(s), 997.87(s), 938.03(m), 911.36(m), 868.29(w), 847.75(w), 778.76(w).

Preparation of Complex ***2***. Complex **2** was prepared in a similar procedure as described for **1** except 0.0124 g (0.2 mmol) of ammonium azide was used as a linker. The immediate precipitation was dissolved by adjusting the pH to 8 by dilute HCl and ammonia. Blue crystals were obtained and dried in the air. Yield: 20% based on **L**^{1}. Elemental analysis (%) Calcd for $C_{16}H_{44}N_{28}O_4Ni_4$: C 21.60, H 3.59, N 42.91. Found: C 21.57, H 4.03, N 42.86. IR, KBr(cm^{-1}): 3278.39(wb), 2867.87(wb), 2064.55($\upsilon_{N_3^-}$,s), 1596.37(s,$\upsilon_{C=N}$),

DOI: 10.1021/acs.cgd.5b00736
Cryst. Growth Des. 2015, 15, 4132−4141

1287.68(w), 1118.92(m), 1083.64(m), 1054.95(w), 995.54(s), 914.44(w), 850.81(w).

Preparation of Complex **3**. A similar procedure as described for **1** was followed using 0.019 g (0.1 mmol) of ammonium salt of BDC as a linker in heating conditions. Dark blue crystals were obtained and dried in air. Yield: 25% based on L^1. Elemental analysis (%) Calcd for $C_{64}H_{164}O_{56}N_{20}Ni_8$: C 30.61, H 3.92, N 11.25. Found: C 30.59, H 3.89, N 11.23. IR, KBr(cm^{-1}): 3350.64(bs), 2925.92(b), 2860.08(b), 2372.57(s), 1569.93($\upsilon_{C\text{-}Oassym\ str.}$, s), 1375.86($\upsilon_{C\text{-}Osym\ str.}$s), 1120.92(w), 998.12(w), 747.48(w) .

Preparation of Complex **4**. Complex **4** was also prepared following the same procedure described above using ammonium salt of NDS as linker (0.0260 g, 0.01 mmol), and the pH of the solution was adjusted to 8 with HCl/NH_3. Dark blue crystals were obtained and dried in air. Yield: 10% based on L^1. Elemental analysis (%) Calcd for $C_{36}H_{80}O_{29}N_{10}Ni_4S_4$: C 29.82, H 3.61, N 9.62. Found: C 29.51, H 3.82, N 9.54. IR, KBr(cm^{-1}): 3449.36($\upsilon_{OH\ str.}$,m), 2946.50(w), 2378.60(b), 1631.36(m.), 1519.38(w), 1313.99(w), 1207.44(s), 1160.89($\upsilon_{sulfonate}$,s), 1046.98($\upsilon_{sulfonate\ bending}$, m), 1031.23(s), 788.18(w)., 769.70(w), 610.25(s), 576.73(w), 527.34(w).

Crystal Structure Determination. All the single crystal data were collected on a Bruker-APEX-II CCD X-ray diffractometer, which uses graphite monochromated Mo Kα radiation (λ = 0.71073 Å) at room temperature (293 K) for complexes **1** and **4** and at low temperature (100 K) for complexes **2** and **3** by the hemisphere method. The structures were solved by direct methods and refined by least-squares methods on F^2 using SHELX-97.[69] Non-hydrogen atoms were refined anisotropically, and hydrogen atoms were fixed at calculated positions and refined using a riding model

■ ASSOCIATED CONTENT

Supporting Information

FT-IR spectra of the complexes **1**−**4**, TGA thermograms for the complexes **1**−**3**, calculated and experimental PXRD patterns for the complexes **1**−**3**, DRS for the complexes **1**−**3**, *M* vs *H* plots and Curie−Weiss plots of complexes **1**−**3**, and proposed reaction mechanism for the formation of **L**. The Supporting Information is available free of charge on the ACS Publications website at DOI: 10.1021/acs.cgd.5b00736.

■ AUTHOR INFORMATION

Corresponding Author

*Fax: +91-3222-282252. Tel: +91-3222-283346. E-mail: kbiradha@chem.iitkgp.ernet.in.

Notes

The authors declare no competing financial interest.

■ ACKNOWLEDGMENTS

We acknowledge DST, New Delhi, India, for financial support and DST-FIST for the single crystal X-ray diffractometer, and D.D. acknowledges UGC for a research fellowship. D.D. is also thankful to Mr. Soumava Biswas, Department of Chemistry, IISER Bhopal, for helping with magnetic data.

■ REFERENCES

(1) Moulton, B.; Zaworotko, M. J. *Chem. Rev.* **2001**, *101*, 1629−1658.
(2) Braga, D.; Grepioni, F.; Desiraju, G. R. *Chem. Rev.* **1998**, *98*, 1375−1406.
(3) Biradha, K.; Sarkar, M.; Rajput, L. *Chem. Commun.* **2006**, *40*, 4169−4179.
(4) Li, J. R.; Kuppler, R. J.; Zhou, H. C. *Chem. Soc. Rev.* **2009**, *38*, 1477−1504.
(5) Li, J. R.; Ma, Y.; McCarthy, M. C.; Sculley, J.; Yu, J.; Jeong, H. K.; Balbuena, P. B.; Zhou, H. C. *Coord. Chem. Rev.* **2011**, *255*, 1791−1823.
(6) Figuerola, A.; Diaz, C.; Ribas, J.; Tangoulis, V.; Sangregorio, C.; Gatteschi, D.; Maestro, M.; Mahía, J. *Inorg. Chem.* **2003**, *42*, 5274−5281.
(7) Batten, S. R.; Murray, K. S. *Coord. Chem. Rev.* **2003**, *246*, 103−130.
(8) Ford, P. C.; Cariati, E.; Bourassa, J. *Chem. Rev.* **1999**, *99*, 3625−3647.
(9) Banerjee, K.; Roy, S.; Biradha, K. *Cryst. Growth Des.* **2014**, *14*, 5164−5170.
(10) Roy, S.; Katiyar, A. K.; Mondal, S. P.; Ray, S. K.; Biradha, K. *ACS Appl. Mater. Interfaces* **2014**, *6*, 11493−11501.
(11) Haldar, R.; Matsuda, R.; Kitagawa, S.; George, S. J.; Maji, T. K. *Angew. Chem., Int. Ed.* **2014**, *53*, 11772−11777.
(12) Chen, C. T.; Suslick, K. S. *Coord. Chem. Rev.* **1993**, *128*, 293−322.
(13) Steed, J. W. *Chem. Soc. Rev.* **2009**, *38*, 506−519.
(14) Bagai, R.; Christou, G. *Chem. Soc. Rev.* **2009**, *38*, 1011−1026.
(15) Cornia, A.; Mannini, M.; Sainctavit, P.; Sessoli, R. *Chem. Soc. Rev.* **2011**, *40*, 3076−3091.
(16) Lee, S. C.; Holm, R. H. *Chem. Rev.* **2004**, *104*, 1135−1158.
(17) Evangelisti, M.; Brechin, E. K. *Dalton Trans.* **2010**, *39*, 4672−4676.
(18) Biswas, S.; Jena, H. S.; Adhikary, A.; Konar, S. *Inorg. Chem.* **2014**, *53*, 3926−3928.
(19) Ama, T.; Rashid, M. M.; Yonemura, T.; Kawaguchi, H.; Yasui, T. *Coord. Chem. Rev.* **2000**, *198*, 101−116.
(20) Matthews, C. J.; Avery, K.; Xu, Z.; Thompson, L. K.; Zhao, L.; Miller, D. O.; Biradha, K.; Poirier, K.; Zaworotko, M. J.; Wilson, C.; et al. *Inorg. Chem.* **1999**, *38*, 5266−5276.
(21) Zhou, Y. L.; Zeng, M. H.; Liu, X. C.; Liang, H.; Kurmoo, M. *Chem. - Eur. J.* **2011**, *17*, 14084−14093.
(22) Isele, K.; Gigon, F.; Williams, A. F.; Bernardinelli, G.; Franz, P.; Decurtins, S. *Dalton trans.* **2007**, *3*, 332−341.
(23) Tong, M. L.; Zheng, S. L.; Shi, J. X.; Tong, Y. X.; Lee, H. K.; Chen, X. M. *J. Chem. Soc., Dalton Trans.* **2002**, *8*, 1727−1734.
(24) Escuer, A.; Aromí, G. *Eur. J. Inorg. Chem.* **2006**, *2006*, 4721−4736.
(25) Manca, G.; Cano, J.; Ruiz, E. *Inorg. Chem.* **2009**, *48*, 3139−3144.
(26) Clemente-Juan, J. M.; Chansou, B.; Donnadieu, B.; Tuchagues, J. P. *Inorg. Chem.* **2000**, *39*, 5515−5519.
(27) Serna, Z.; De la Pinta, N.; Urtiaga, M. K.; Lezama, L.; Madariaga, G.; Clemente-Juan, J. M.; Coronado, E.; Cortés, R. *Inorg. Chem.* **2010**, *49*, 11541−11549.
(28) Barandika, M. G.; Cortes, R.; Serna, Z.; Lezama, L.; Rojo, T.; Urtiaga, M. K.; Arriortua, M. I. *Chem. Commun.* **2001**, *1*, 45−46.
(29) Youngme, S.; Phatchimkun, J.; Suksangpanya, U.; Pakawatchai, C.; van Albada, G. A.; Quesada, M.; Reedijk, J. *Inorg. Chem. Commun.* **2006**, *9*, 242−247.
(30) Lin, Z.; Li, Z.; Zhang, H. *Cryst. Growth Des.* **2007**, *7*, 589−591.
(31) Subramanian, S.; Zaworotko, M. J. *Angew. Chem., Int. Ed. Engl.* **1995**, *34*, 2127−2129.
(32) Wang, S.; Ding, X. H.; Zuo, J. L.; You, X. Z.; Huang, W. *Coord. Chem. Rev.* **2011**, *255*, 1713−1732.
(33) Zhao, D.; Timmons, D. J.; Yuan, D. Q.; Zhou, H. C. *Acc. Chem. Res.* **2011**, *44*, 123−133.
(34) O'Keeffe, M.; Yaghi, O. M. *Chem. Rev.* **2012**, *112*, 675−702.
(35) Roy, S.; Mahata, G.; Biradha, K. *Cryst. Growth Des.* **2009**, *9*, 5006−5008.
(36) Thallapally, P. K.; Chakraborty, K.; Katz, A. K.; Carrell, H. L.; Kotha, S.; Desiraju, G. R. *CrystEngComm* **2001**, *3*, 134−136.
(37) Santra, R.; Ghosh, N.; Biradha, K. *New J. Chem.* **2008**, *32*, 1673−1676.
(38) Santra, R.; Biradha, K. *Cryst. Growth Des.* **2009**, *9*, 4969−4978.
(39) Mukherjee, G.; Biradha, K. *Cryst. Growth Des.* **2014**, *14*, 419−422.
(40) Hazra, S.; Sarkar, B.; Naiya, S.; Drew, M. G. B.; Ribas, J.; Diaz, C.; Ghosh, A. *Inorg. Chem. Commun.* **2011**, *14*, 1860−1863.
(41) Allen, F. H. *Acta Crystallogr., Sect. B: Struct. Sci.* **2002**, *B58*, 380−388.

DOI: 10.1021/acs.cgd.5b00736
Cryst. Growth Des. 2015, 15, 4132−4141

(42) Murray-Rust, P. *J. Chem. Soc., Perkin Trans. 2* **1974**, *10*, 1136−1141.
(43) Rivera, A.; Gonzalez-Salas, D.; Rios-Motta, J.; Hernandez-Barragan, A.; Joseph-Nathan, P. *J. Mol. Struct.* **2007**, *837*, 142−146.
(44) Rivera, A.; Torres, O. L.; Leitón, J. D.; Morales-Ríos, M. S.; Joseph-Nathan, P. *Synth. Commun.* **2002**, *32*, 1407−1414.
(45) Glister, J. F.; Vaughan, K.; Biradha, K.; Zaworotko, M. J. *J. Mol. Struct.* **2005**, *749*, 78−83.
(46) Sudik, A. C.; Côté, A. P.; Yaghi, O. M. *Inorg. Chem.* **2005**, *44*, 2998−3000.
(47) Lan, Y. Q.; Wang, X. L.; Li, S. L.; Su, Z. M.; Shao, K. Z.; Wang, E. B. *Chem. Commun.* **2007**, 4863−4865.
(48) Hou, L.; Lin, Y.; Chen, X. M. *Inorg. Chem.* **2008**, *47*, 1346−1351.
(49) Yang, E.; Liu, Z. S.; Lin, S.; Chen, S. Y. *Inorg. Chem. Commun.* **2011**, *14*, 1588−1590.
(50) Li, X. J.; Wang, X. Y.; Gao, S.; Cao, R. *Inorg. Chem.* **2006**, *45*, 1508−1516.
(51) Donlevy, T. M.; Gahan, L. R.; Stranger, R.; Kennedy, S. E.; Byriel, K. A.; Kennard, C. H. L *Inorg. Chem.* **1993**, *32*, 6023−6027.
(52) Wikstrom, J. P.; Nazarenko, A. Y.; Reiff, W. M.; Rybak-Akimova, E. V. *Inorg. Chim. Acta* **2007**, *360*, 3733−3740.
(53) Meyer, A.; Gleizes, Al.; Girerd, J. J.; Verdaguer, M.; Kahn, O. *Inorg. Chem.* **1982**, *21*, 1729−1739.
(54) Herchel, R.; Boča, R.; Krzystek, J.; Ozarowski, A.; Durán, M.; van Slageren, J. *J. Am. Chem. Soc.* **2007**, *129*, 10306−10307.
(55) Ponomaryov, A. N.; Kim, N.; Hwang, J.; Nojiri, H.; Tol, J. V.; Ozarowski, A.; Park, J.; Jang, Z.; Suh, B.; Yoon, B.; Choi, K. Y. *Chem. - Asian J.* **2013**, *8*, 1152−1159.
(56) Packová, A.; Miklovič, J.; Titiš, J.; Koman, M.; Boča, R. *Inorg. Chem. Commun.* **2013**, *32*, 9−11.
(57) Halcrow, M. A.; Sun, J. S.; Huffman, J. C.; Christou, G. *Inorg. Chem.* **1995**, *34*, 4167−4177.
(58) Breeze, B. A.; Shanmugam, M.; Tuna, F.; Winpenny, R. E. P. *Chem. Commun.* **2007**, 5185−5187.
(59) Hong, C. S.; Koo, J. E.; Son, S. K.; Lee, Y. S.; Kim, Y. S.; Do, Y. *Chem. - Eur. J.* **2001**, *7*, 4243−4252.
(60) Serna, Z. F.; Lezama, L.; Urtiaga, M. K.; Arriortua, M. I.; Barandika, M. G.; Cortes, R.; Rojo, T. *Angew. Chem., Int. Ed.* **2000**, *39*, 344−347.
(61) Ribas, J.; Escuer, A.; Monfort, M.; Vicente, R.; Cortés, R.; Lezama, L.; Rojo, T. *Coord. Chem. Rev.* **1999**, *193-195*, 1027−1068.
(62) Cano, J.; De Munno, G.; Sanz, J.; Ruiz, R.; Lloret, F.; Faus, J.; Julve, M. *J. Chem. Soc., Dalton Trans.* **1994**, *23*, 3465−3469.
(63) Nytko, E. A.; Helton, J. S.; Mueller, P.; Nocera, D. G. *J. Am. Chem. Soc.* **2008**, *130*, 2922−2923.
(64) Manna, S. C.; Konar, S.; Zangrando, E.; Okamoto, K.; Ribas, J.; Chaudhuri, N. R. *Eur. J. Inorg. Chem.* **2005**, No. 22, 4646−4654.
(65) Kurmoo, M.; Kumagai, H.; Green, M. A.; Lovett, B. W.; Blundell, S. J.; Ardavan, A.; Singleton, J. *J. Solid State Chem.* **2001**, *159*, 343−351.
(66) Kickelbick, G.; Rutzinger, D.; Gallauner, T. *Monatsh. Chem.* **2002**, *133*, 1157−1164.
(67) Köhn, R. D.; Haufe, M.; Kociok-Köhn, G.; Filippou, A. C. *Inorg. Chem.* **1997**, *36*, 6064−6069.
(68) Kahn, O. *Molecular Magnetism*; VCH: New York, 1993.
(69) Sheldrick, G. M. SHELX-97, Program for the Solution and Refinement of Crystal Structures; University of Göttingen: Germany, 1997.

DOI: 10.1021/acs.cgd.5b00736
Cryst. Growth Des. 2015, 15, 4132−4141